LA-UR-01-3630
Approved for public release;
distribution is unlimited.

Title: **A Cylindrically Symmetric Uniaxial PML Maxwell Solver for Transient Atmospheric Electricity Simulations**

Author(s): Eugene M. D. Symbalisty

Submitted to:

http://lib-www.lanl.gov/la-pubs/00796218.pdf

A Cylindrically Symmetric Uniaxial PML Maxwell Solver for Transient Atmospheric Electricity Simulations

Eugene M. D. Symbalisty

1 Introduction

The recent interest in high altitude discharges known as red sprites, blue jets, and elves has stimulated the modeling of transient atmospheric electricity. The modeling of these high altitude discharges require an initiating cloud-to-ground or intracoud lightning event in order to pre-condition the electric field between the cloud tops and the ionosphere. In this short paper we describe a finite difference time domain (FDTD) numerical solution of Maxwell's equations based on the Yee (Yee 1966) algorithm coupled with a uniaxial perfectly matched layer (PML, Berenger 1994) boundary treatment. The PML theory has advanced considerably since its original formulation in cartesian coordinates for lossless media, and is computationally efficient to implement. Another boundary treatment possibility for our sources that produce radiative and electrostatic fields, which we do not consider here, is a multipole expansion in the time domain for the electromagnetic fields.

This treatment borrows heavily from the texts of Taflove (1995 and 1998), Sullivan (2000), and Taflove and Hagness (2000). However, the particular equation set of interest, as far as we know, has not been described in detail elsewhere. We write Maxwell's equations as follows:

$$\frac{\partial \mathbf{B}}{\partial t} = -\nabla \times \mathbf{E}, \quad \frac{\partial \mathbf{D}}{\partial t} = \nabla \times \mathbf{H} - \mathbf{J} \tag{1}$$

$$\mathbf{B} = \mu \mathbf{H} = \mu_r \mu_0 \mathbf{H}, \quad \mathbf{D} = \epsilon \mathbf{E} = \epsilon_r \epsilon_0 \mathbf{E}, \quad \mathbf{J} = \sigma \mathbf{E} + \mathbf{J}_s \tag{2}$$

The current term is split into an ohmic term and a source term, $\mathbf{J}_s$. The source term may represent, for example, an intracloud lightning or cloud-to-ground lightning event.

The paper is organized as follows. Maxwell's equations are written in the frequency domain including the PML boundary treatment. Maxwell's equations are then rewritten in the time domain including the terms for the PML boundary treatment. The FDTD numerical solution is then written down. Test problems are then descibed. The test problems are relevant to the initiating lightning event and therefore charged regions, radiative and electrostatic fields evolve from an impulsive current source. The test problems consist of running the same current source on a large and small grid. The final time is chosen when the electromagnetic wave is about to impinge upon a PML boundary on the large grid. The large grid numerical solution is considered to be the *true* solution. The small grid is chosen such that any numerical reflections off the small grid boundaries will have had time to propagate back through the entire grid by the final time. The small grid and true solutions are then compared and a relative error is computed.

2 Frequency Domain Equation Set

We begin with Maxwell's curl equations in a uniaxial medium (Taflove 1998, p.330) in cylindrical coordinates:

$$\nabla \times \mathbf{H} - \mathbf{J}_s = j\omega\epsilon_o(\epsilon_r + \frac{\sigma}{j\omega\epsilon_o}) \ \bar{\bar{S}}_c \ \mathbf{E} \tag{3}$$

$$-\nabla \times \mathbf{E} = j\omega\mu_o\mu_r \ \bar{\bar{S}}_c \ \mathbf{H} \tag{4}$$

$$\bar{\bar{S}}_c = \begin{pmatrix} \frac{s_z}{s_\rho}\frac{\hat{\rho}}{\rho} & 0 & 0 \\ 0 & s_z s_\rho \frac{\rho}{\hat{\rho}} & 0 \\ 0 & 0 & \frac{s_\rho}{s_z}\frac{\hat{\rho}}{\rho} \end{pmatrix} \tag{5}$$

We now specialize to our two dimensional axisymmetric (around the $\rho = 0$ axis) case. We are evolving E_ρ, E_z, and H_ϕ and all derivatives with respect to ϕ are set to zero. Therefore, the above six equations for $\mathbf{E}$ and $\mathbf{H}$ reduce to the following three:

$$j\omega\epsilon_o(\epsilon_r + \frac{\sigma}{j\omega\epsilon_o})\frac{s_z}{s_\rho}\frac{\hat{\rho}}{\rho}E_\rho = [\nabla \times \mathbf{H} - \mathbf{J}_s]_\rho \equiv C_\rho \tag{6}$$

$$jw\omega\epsilon_o(\epsilon_z + \frac{\sigma}{j\omega\epsilon_o})\frac{s_\rho}{s_z}\frac{\hat{\rho}}{\rho}E_z = [\nabla \times \mathbf{H} - \mathbf{J}_s]_z \equiv C_z \tag{7}$$

$$j\omega\mu_o\mu_r s_\rho s_z \frac{\rho}{\hat{\rho}}H_\phi = [-\nabla \times \mathbf{E}]_\phi \equiv C_\phi \tag{8}$$

where the PML boundary functions are defined as

$$s_\rho = \kappa_\rho + \frac{\sigma_\rho}{j\omega\epsilon_o} \tag{9}$$

$$s_z = \kappa_z + \frac{\sigma_z}{j\omega\epsilon_o} \tag{10}$$

$$\frac{\hat{\rho}}{\rho} = \begin{cases} \kappa_\rho & \text{for } \rho \le \rho_0 \\ \kappa_\rho + \frac{1}{j\omega\rho\epsilon_o}\int_{\rho_o}^{\rho}\sigma_\rho(\rho')d\rho' & \text{for } \rho > \rho_o \end{cases} \tag{11}$$

$$\sigma_\rho = \begin{cases} 0 & \text{for } \rho \le \rho_0 \\ \sigma_m \ (\frac{\rho-\rho_o}{\rho_m-\rho_o})^m & \text{for } \rho > \rho_o \end{cases} \tag{12}$$

$$\sigma_z = \begin{cases} 0 & \text{for } z_1 \le z \le z2 \\ \sigma_m \ (\frac{z_1-z}{z_1-z_b})^m & \text{for } z < z_1 \\ \sigma_m \ (\frac{z-z_2}{z_t-z_2})^m & \text{for } z > z_2 \end{cases} \tag{13}$$

$$\kappa_\rho = \begin{cases} 1 & \text{for } \rho \le \rho_0 \\ 1 + (\kappa_m - 1) \ (\frac{\rho-\rho_o}{\rho_m-\rho_o})^m & \text{for } \rho > \rho_o \end{cases} \tag{14}$$

$$\kappa_z = \begin{cases} 1 & \text{for } z_1 \le z \le z_2 \\ 1 + (\kappa_m - 1)\ (\frac{z_1 - z}{z_1 - z_b})^m & \text{for } z < z_1 \\ 1 + (\kappa_m - 1)\ (\frac{z - z_2}{z_t - z_2})^m & \text{for } z > z_2 \end{cases} \tag{15}$$

The PML boundary zones: (1) in the radial direction begin at ρ_o and extend to the maximum radius of the grid ρ_m; (2) in the positive z direction begin at z_2 and extend to the top of the grid z_t, and ; (3) in the negative z direction extend from z_1 down to the bottom of the grid z_b. They are backed by a perfect electrical conductor (PEC).

The parameters κ_ρ and κ_z are designed to kill outgoing evanescent waves when set to a value greater than 1. Thus far, in our studies of atmospheric electricity, these waves have not presented a problem and we therefore set the input parameter κ_m equal to one.

The parameter σ_m is the maximum artifical conductivity in the PML zones. If d is the overall length of the PML region in a given direction then, following Taflove (1995), we set

$$\sigma_m = -\frac{(m+1) ln R_o}{2\epsilon_r d\sqrt{\mu/\epsilon}} \equiv \frac{(m+1)\chi}{2\epsilon_r d\sqrt{\mu/\epsilon}} \tag{16}$$

R_o is the theorectical reflection coefficient at normal incidence, which we set equal to $e^{-\chi}$. The test problems described in a following section used $\chi = 10$, $m = 3$, and 16 PML boundary zones at each PML boundary. Following Taflove (1998), we next define

$$P_\rho = \frac{1}{s_\rho}\frac{\hat{\rho}}{\rho}E_\rho, \qquad P_z = \frac{1}{s_z}\frac{\hat{\rho}}{\rho}E_z \tag{17}$$

$$Q_\rho = s_z P_\rho, \qquad Q_z = s_\rho P_z, \qquad Q_\phi = s_z \frac{\rho}{\hat{\rho}} H_\phi \tag{18}$$

Eight frequency domain equations can now be written down, after some algebra, as follows

$$j\omega\epsilon_r Q_\rho + \frac{\sigma}{\epsilon_o}Q_\rho = \frac{C_\rho}{\epsilon_o} \tag{19}$$

$$j\omega\epsilon_r Q_z + \frac{\sigma}{\epsilon_o}Q_z = \frac{C_z}{\epsilon_o} \tag{20}$$

$$j\omega\kappa_\rho Q_\phi + \frac{\sigma_\rho}{\epsilon_o}Q_\phi = \frac{C_\phi}{\mu_o\mu_r} \tag{21}$$

$$j\omega\kappa_z P_\rho + \frac{\sigma_z}{\epsilon_o}P_\rho = j\omega Q_\rho \tag{22}$$

$$j\omega\kappa_\rho P_z + \frac{\sigma_\rho}{\epsilon_o}P_z = j\omega Q_z \tag{23}$$

$$j\omega\kappa_\rho E_\rho + \frac{S}{\rho\epsilon_o}E_\rho = j\omega\kappa_\rho P_\rho + \frac{\sigma_\rho}{\epsilon_o}P_\rho \tag{24}$$

$$j\omega\kappa_\rho E_z + \frac{S}{\rho\epsilon_o}E_z = j\omega\kappa_z P_z + \frac{\sigma_z}{\epsilon_o}P_z \tag{25}$$

$$j\omega\kappa_z H_\phi + \frac{\sigma_z}{\epsilon_o} H_\phi = j\omega\kappa_\rho Q_\phi + \frac{S}{\rho\epsilon_o} Q_\phi \tag{26}$$

where

$$S = \begin{cases} 0 & \text{for } \rho \leq \rho_o \\ \int_{\rho_o}^{\rho} \sigma_\rho(\rho') d\rho' & \text{for } \rho > \rho_o \end{cases} \tag{27}$$

3 Time Domain Equation Set

Equations 19 through 26 are now easily converted to the time domain. We obtain:

$$\frac{\partial(\epsilon_r Q_\rho)}{\partial t} + \frac{\sigma}{\epsilon_o} Q_\rho = \frac{C_\rho}{\epsilon_o} \tag{28}$$

$$\frac{\partial(\epsilon_r Q_z)}{\partial t} + \frac{\sigma}{\epsilon_o} Q_z = \frac{C_z}{\epsilon_o} \tag{29}$$

$$\frac{\partial(\kappa_\rho Q_\phi)}{\partial t} + \frac{\sigma_\rho}{\epsilon_o} Q_\phi = \frac{C_\phi}{\mu_o \mu_r} \tag{30}$$

$$\frac{\partial(\kappa_z P_\rho)}{\partial t} + \frac{\sigma_z}{\epsilon_o} P_\rho = \frac{\partial Q_\rho}{\partial t} \tag{31}$$

$$\frac{\partial(\kappa_\rho P_z)}{\partial t} + \frac{\sigma_\rho}{\epsilon_o} P_z = \frac{\partial Q_z}{\partial t} \tag{32}$$

$$\frac{\partial(\kappa_\rho E_\rho)}{\partial t} + \frac{S}{\rho\epsilon_o} E_\rho = \frac{\partial(\kappa_\rho P_\rho)}{\partial t} + \frac{\sigma_\rho}{\epsilon_o} P_\rho \tag{33}$$

$$\frac{\partial(\kappa_\rho E_z)}{\partial t} + \frac{S}{\rho\epsilon_o} E_z = \frac{\partial(\kappa_z P_z)}{\partial t} + \frac{\sigma_z}{\epsilon_o} P_z \tag{34}$$

$$\frac{\partial(\kappa_z H_\phi)}{\partial t} + \frac{\sigma_z}{\epsilon_o} H_\phi = \frac{\partial(\kappa_\rho Q_\phi)}{\partial t} + \frac{S}{\rho\epsilon_o} Q_\phi \tag{35}$$

4 Numerical Solution

Equations 28 and equation 29 are the only two of the time dependent equation set that include the time and altitude dependent ambient electrical conductivity. In order to allow for rapid and large increases in this conductivity they are solved with exponential time stepping (Taflove 1995). We have:

$$Q_\rho(t + \Delta t) = Q_\rho(t)\ e^{-\frac{\sigma}{\epsilon}\Delta t} + \frac{C_\rho^{n+\frac{1}{2}}}{\sigma}(1 - e^{-\frac{\sigma}{\epsilon}\Delta t}) \tag{36}$$

$$Q_z(t + \Delta t) = Q_z(t)\ e^{-\frac{\sigma}{\epsilon}\Delta t} + \frac{C_z^{n+\frac{1}{2}}}{\sigma}(1 - e^{-\frac{\sigma}{\epsilon}\Delta t}) \tag{37}$$

The remaining equations are written down in a straight forward FDTD approximation, following Taflove (1998) and allowing for time centering:

$$Q_\phi^{n+1/2}(\kappa_\rho + \frac{\sigma_\rho \Delta t}{2\epsilon_o}) = Q_\phi^{n-1/2}(\kappa_\rho - \frac{\sigma_\rho \Delta t}{2\epsilon_o}) + \frac{C_\phi^n \Delta t}{\mu} \tag{38}$$

$$P_\rho^{n+1}(\kappa_z + \frac{\sigma_z \Delta t}{2\epsilon_o}) = P_\rho^n(\kappa_z - \frac{\sigma_z \Delta t}{2\epsilon_o}) + (Q_\rho^{n+1} - Q_\rho^n) \tag{39}$$

$$P_z^{n+1}(\kappa_\rho + \frac{\sigma_\rho \Delta t}{2\epsilon_o}) = P_z^n(\kappa_\rho - \frac{\sigma_\rho \Delta t}{2\epsilon_o}) + (Q_z^{n+1} - Q_z^n) \tag{40}$$

$$E_\rho^{n+1}(\kappa_\rho + \frac{S\Delta t}{2\epsilon_o \rho}) = E_\rho^n(\kappa_\rho - \frac{S\Delta t}{2\epsilon_o \rho}) + P_\rho^{n+1}(\kappa_\rho + \frac{\sigma_\rho \Delta t}{2\epsilon_o}) - P_\rho^n(\kappa_\rho - \frac{\sigma_\rho \Delta t}{2\epsilon_o}) \tag{41}$$

$$E_z^{n+1}(\kappa_\rho + \frac{S\Delta t}{2\epsilon_o \rho}) = E_z^n(\kappa_\rho - \frac{S\Delta t}{2\epsilon_o \rho}) + P_z^{n+1}(\kappa_z + \frac{\sigma_z \Delta t}{2\epsilon_o}) - P_z^n(\kappa_z - \frac{\sigma_z \Delta t}{2\epsilon_o}) \tag{42}$$

$$H_\phi^{n+\frac{1}{2}}(\kappa_z + \frac{\sigma_z \Delta t}{2\epsilon_o}) = H_\phi^{n-\frac{1}{2}}(\kappa_z - \frac{\sigma_z \Delta t}{2\epsilon_o}) + Q_\phi^{n+\frac{1}{2}}(\kappa_\rho + \frac{S\Delta t}{2\epsilon_o \rho}) - Q_\phi^{n-\frac{1}{2}}(\kappa_\rho - \frac{S\Delta t}{2\epsilon_o \rho}) \tag{43}$$

The relative permeability is assumed to be constant in time in the above equations. The time dependent equations reduce to Maxwell's equations in the real, non-PML zones, and the numerical solution reduces to the Yee algorithm in the real zones.

5 Test Problems

The first problem models an intracloud lightning event with PML boundaries on the right hand, top, and bottom sides. We are careful to invent a current density that has a neglible current in the PML zones. The current density has a vertical component only:

$$J_z(\rho, z, t) = f(t)\ e^{-(\frac{\rho}{a})^2} \begin{cases} 1 & \text{for } z_- \le z \le z_+ \\ e^{-(\frac{z_- - z}{b})^2} & \text{for } z < z_- \\ e^{-(\frac{z - z_+}{b})^2} & \text{for } z > z_+ \end{cases} \tag{44}$$

The altitudes z_+ and z_-, set equal to 2.15 and 1.85 km respectively for this test case, are input parameters and correspond to the centers of the ellipsoidal charge distributions (of opposite sign) that develop. For the tests describe herein, we used a Uman like time dependence for the lightning event, with Q_d being the value of the charge, and τ and β being input parameters:

$$f(t) = \frac{Q_d}{\pi a^2} \frac{\beta}{\tau(\beta - 1)} (e^{-\frac{t}{\tau}} - e^{-\beta \frac{t}{\tau}}) \tag{45}$$

Figure 1 displays the absolute value of the radial and z electric fields and the magnetic field on the large grid just before the electromagnetic wave reaches any of the PML boundaries. Q_D was set to -10 Coulombs. The grid dimensions are in km and the grid cells are 10 m squares. In this case $\tau = 1$ microsecond and $\beta = 3$. Figure 2 displays the absolute value of the z component on the small grid,

the large grid, and the relative error from left to right. The left and middle figures correspond to the middle graphic on figure 1, but zoomed in on the small grid. Actually we are plotting to within 5 cells of the PML boundaries on the small grid. The relative error is defined as:

$$Relative\ \ Error = |(E_{small} - E_{large})/E_{large}| \tag{46}$$

The color bars on the small and large field plots are identical. If the value of field is zero on the large grid then the relative error is not computed. If the relative error is less than the black value of the color bar then it is not plotted and appears as white. We see that the relative error is only large where the field in going through zero and, in fact, is changing sign. Figure 3 is similar to figure 2 except that it is the magnetic field that is displayed. The magnetic field clearly reflects off the right hand side boundary but the relative error is 0.001 or less. The magnetic field is more sensitive in our two tests because the electrostatic field dominates the electric field plots once the radiation field has exited the small grid.

The second problem models a cloud-to-ground lightning event with PML boundaries on the right hand and top side only. The bottom boundary, or ground is set to be a perfect conductor. The altitude z_+ is an input parameter, set equal to 10 km, and corresponds to the altitude where an ellipsoidal charge distribution develops. The grid cells are 500 m and $\tau = 100$ microseconds and $\beta = 3$. We are, again, careful to invent a current density that has a neglible current in the PML zones. The current density is similar to equation 44 except that it draws charge from the ground:

$$J_z(\rho, z, t) = f(t)\ \ e^{-(\frac{\rho}{a})^2} \begin{cases} 1 & \text{for } z \le z_+ \\ e^{-(\frac{z-z_+}{b})^2} & \text{for } z > z_+ \end{cases} \tag{47}$$

Q_d was set to -140 Coulombs. Figure 4 displays the absolute value of the radial and z electric fields and the magnetic field on the large grid just as the electromagnetic wave reaches the right hand side PML boundary. The PML boundary on the top turns out to be irrelevant because the ambient electrical conductivity reduces the field to near zero before entry to the PML region. Figure 5, analagous to figure 2 for the first test case, displays the absolute value of the z component on the small grid, the large grid, and the relative error from left to right. We see that the relative error is, again, only large where the field in going through zero and, in fact, is changing sign. Figure 6, analagous to figure 3 displays the small grid, large grid, and relative error of the magnetic field. In this case the relative error can be quite large as the field goes through zero and changes sign.

We next estimate a grid average relative error as follows:

$$F\ \ error = \frac{\sum |F_{small} - F_{large}|}{\sum |F_{large}|} \tag{48}$$

The symbol F represents one of the electric or magnetic field components. Table 1 tabulates this grid averaged relative error. The summations in equation 48 are over the small grid to within five zones of the PML boundaries.

We performed some numerical simulations varying the number of PML in each direction and also the parameter χ in equation 16. The results are found in table 2. We note that the zero PML zone case corresponds to the perfect reflector boundary conditions and we therefore expect and obtain very large errors. We see that with $\chi = 10$ each error continues to decrease as the number of zones increases. However, we also note that increasing χ from 10 to 16 and keeping the numbers of PML zones constant

Table 1: Grid Average Relative Error

Test	E_z **Error**	E_r **Error**	B_ϕ **Error**
1	2.67×10^{-5}	6.41×10^{-6}	3.42×10^{-4}
2	3.11×10^{-5}	1.57×10^{-5}	6.79×10^{-4}

Table 2: Test 1 Grid Average Relative Error For Different Parameters

PML Zones	χ	E_z **Error**	E_r **Error**	B_ϕ **Error**
0	10	0.365	0.05399	4.93
8	10	1.54×10^{-4}	3.42×10^{-5}	1.99×10^{-3}
12	10	5.81×10^{-5}	1.39×10^{-5}	7.54×10^{-4}
16	10	2.67×10^{-5}	6.41×10^{-6}	3.42×10^{-4}
20	10	1.42×10^{-5}	3.48×10^{-6}	1.80×10^{-4}
24	10	9.20×10^{-6}	2.14×10^{-6}	1.22×10^{-4}
28	10	6.93×10^{-6}	1.41×10^{-6}	9.42×10^{-5}
28	16	1.11×10^{-5}	2.01×10^{-6}	1.50×10^{-4}

at 28 actually increased the error. We suspect that the exact choice for χ, the number of PML zones, and the PML exponent is problem dependent. The exponent was kept at 3 for the work described in this paper.

6 Conclusions

We have derived, beginning with the tensor Maxwell curl equations of Taflove (1998), the frequency domain, time domain, and finite difference equations for problems that satisfy azimuthal symmetry with ohmic and source currents. These problems include two dimensional high altitude discharge studies and intracloud lightning studies. We have demonstrated that a uniaxial PML treatment reduces reflections from boundaries to a suitably small level.

Bibliography

1. Berenger, J. P. *A perfectly matched layer for the absorption of electromagnetic waves*, J. Comp. Physics, Vol. 114, pp.185-200, 1994.

2. Sullivan, D. M. *Electromagnetic Simulation using the FDTD Method*, IEEE press, 2000.

3. Taflove, A., *Computational Electrodynamics*, Artech House, Boston 1995.

4. Taflove, A. editor, *Advances in Computational Electrodynamics*, Artech House, Boston 1998.

5. Taflove, A. and S. Hagness, editors, *Computational Electrodynamics*, Second Edition, Artech House, Boston 2000.

6. Yee, K. S., *Numerical Solution of Initial Boundary Value Problems involving Maxwell's Equation in isotropic media*, IEEE Trans. Antennas and Propagation, Vol. 14, pp. 302-307, 1966.

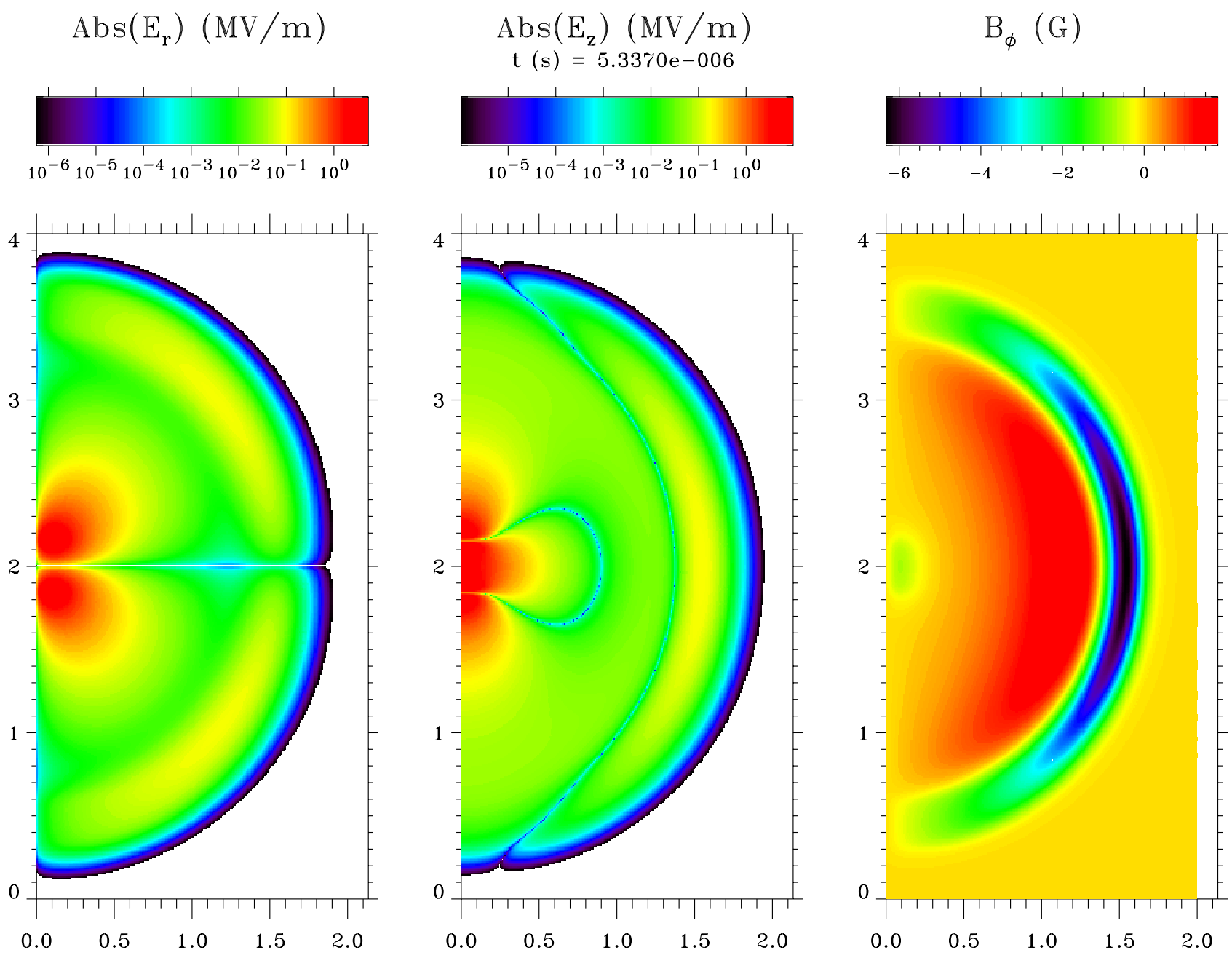
Abs(E_r) (MV/m)
10^-6 10^-5 10^-4 10^-3 10^-2 10^-1 10^0
Abs(E_z) (MV/m)
t (s) = 5.3370e-006
10^-5 10^-4 10^-3 10^-2 10^-1 10^0
B_φ (G)
−6 −4 −2 0
0 1 2 3 4
0.0 0.5 1.0 1.5 2.0

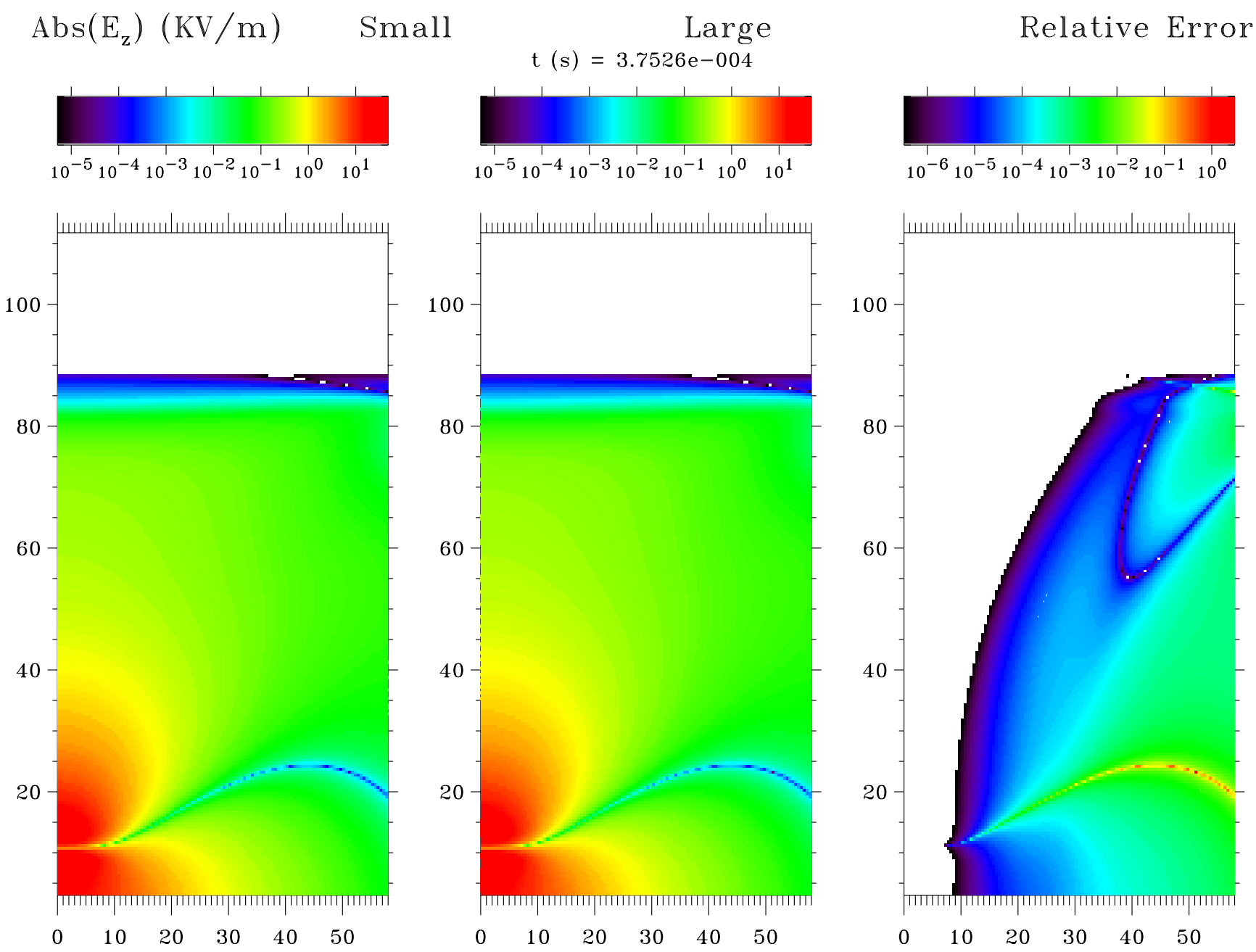
Abs(E_z) (KV/m)
Small
Large
Relative Error
t (s) = 3.7526e-004
10^-5 10^-4 10^-3 10^-2 10^-1 10^0 10^1
10^-5 10^-4 10^-3 10^-2 10^-1 10^0 10^1
10^-6 10^-5 10^-4 10^-3 10^-2 10^-1 10^0
100
80
60
40
20
0 10 20 30 40 50

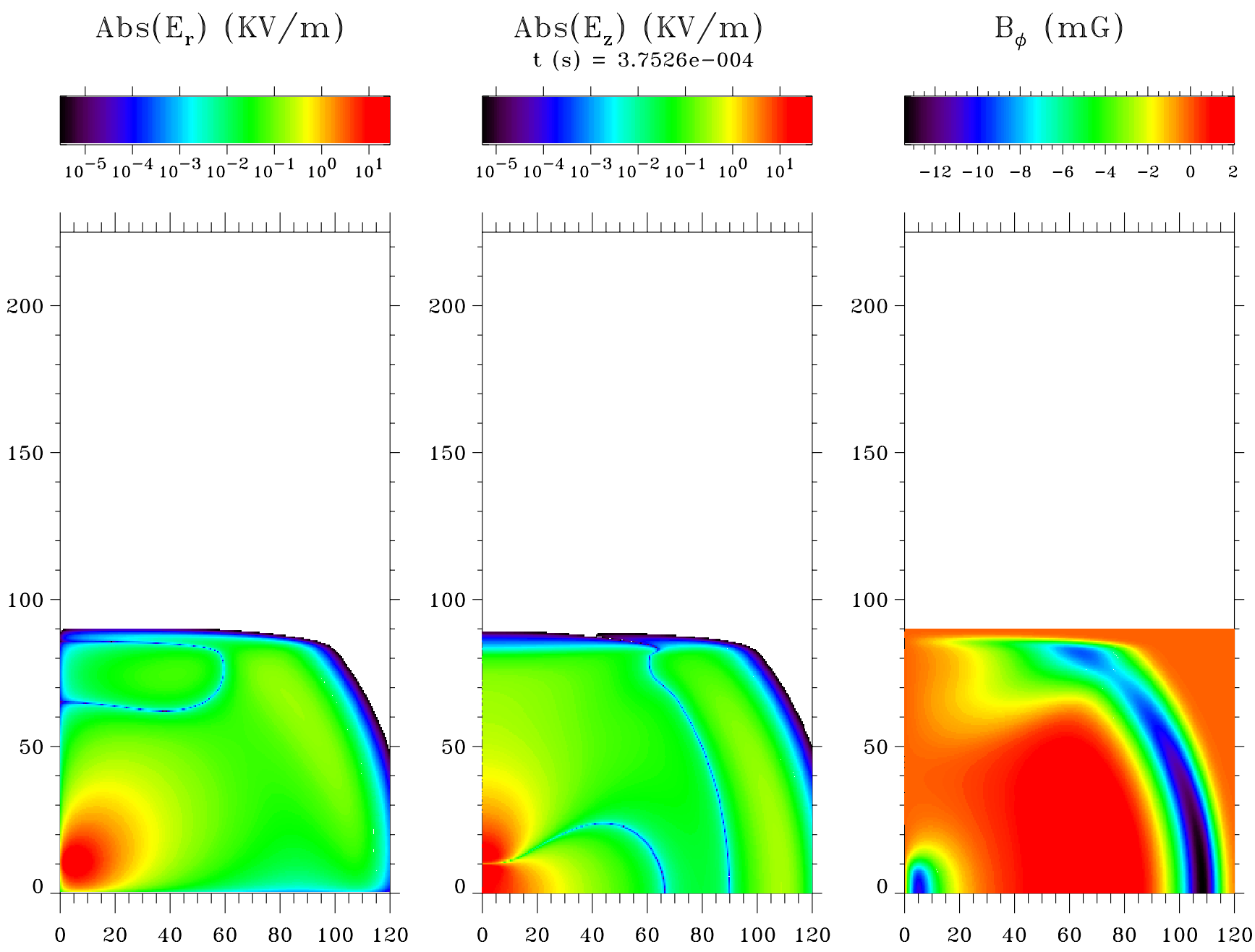
Abs(E_r) (KV/m)
Abs(E_z) (KV/m)
t (s) = 3.7526e−004
B_φ (mG)
10^−5 10^−4 10^−3 10^−2 10^−1 10^0 10^1
10^−5 10^−4 10^−3 10^−2 10^−1 10^0 10^1
−12 −10 −8 −6 −4 −2 0 2
200
150
100
50
0
0 20 40 60 80 100 120
0 20 40 60 80 100 120
0 20 40 60 80 100 120

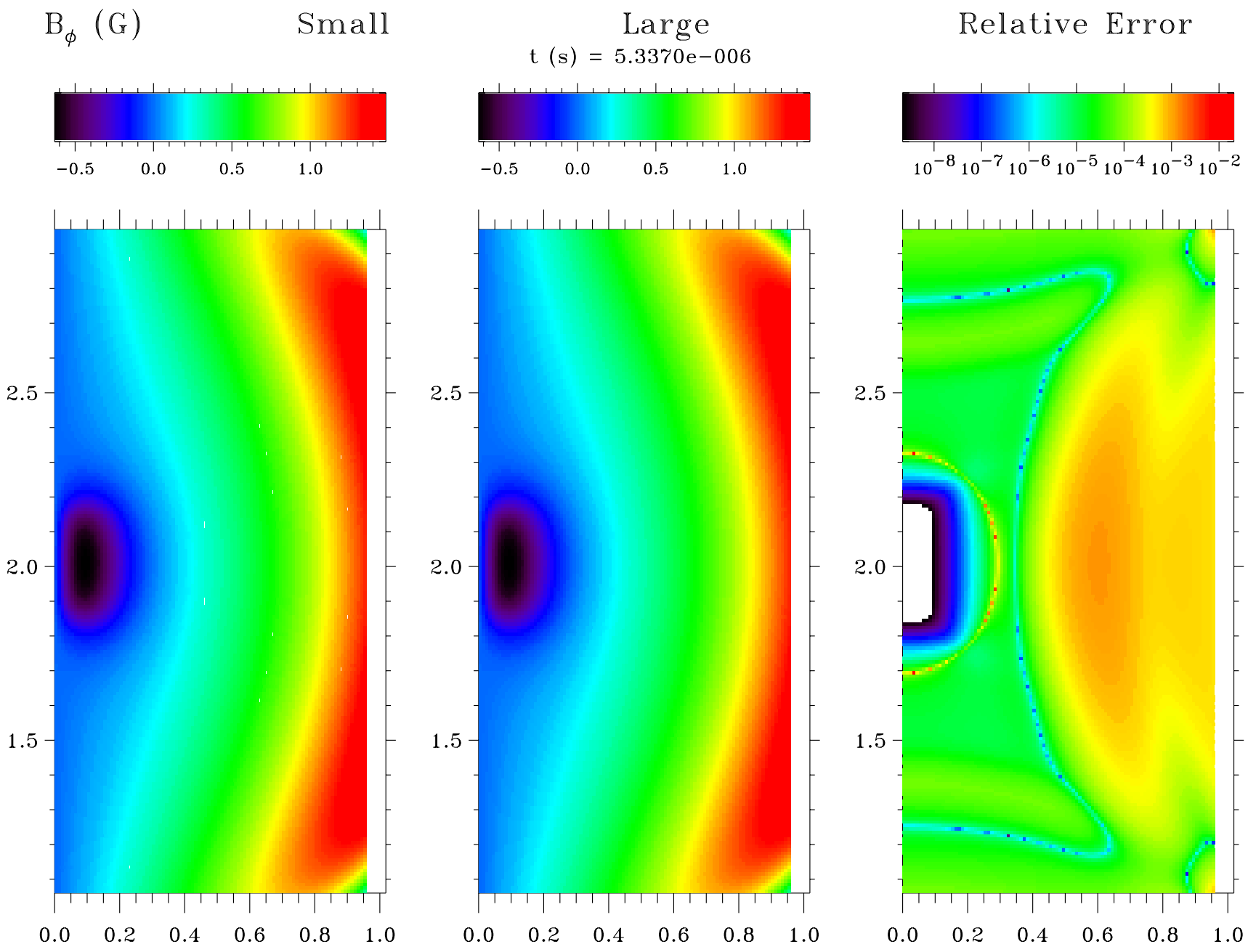
B_ϕ (G)
Small
Large
t (s) = 5.3370e−006
Relative Error
−0.5 0.0 0.5 1.0
−0.5 0.0 0.5 1.0
10^{-8} 10^{-7} 10^{-6} 10^{-5} 10^{-4} 10^{-3} 10^{-2}
2.5
2.0
1.5
0.0 0.2 0.4 0.6 0.8 1.0

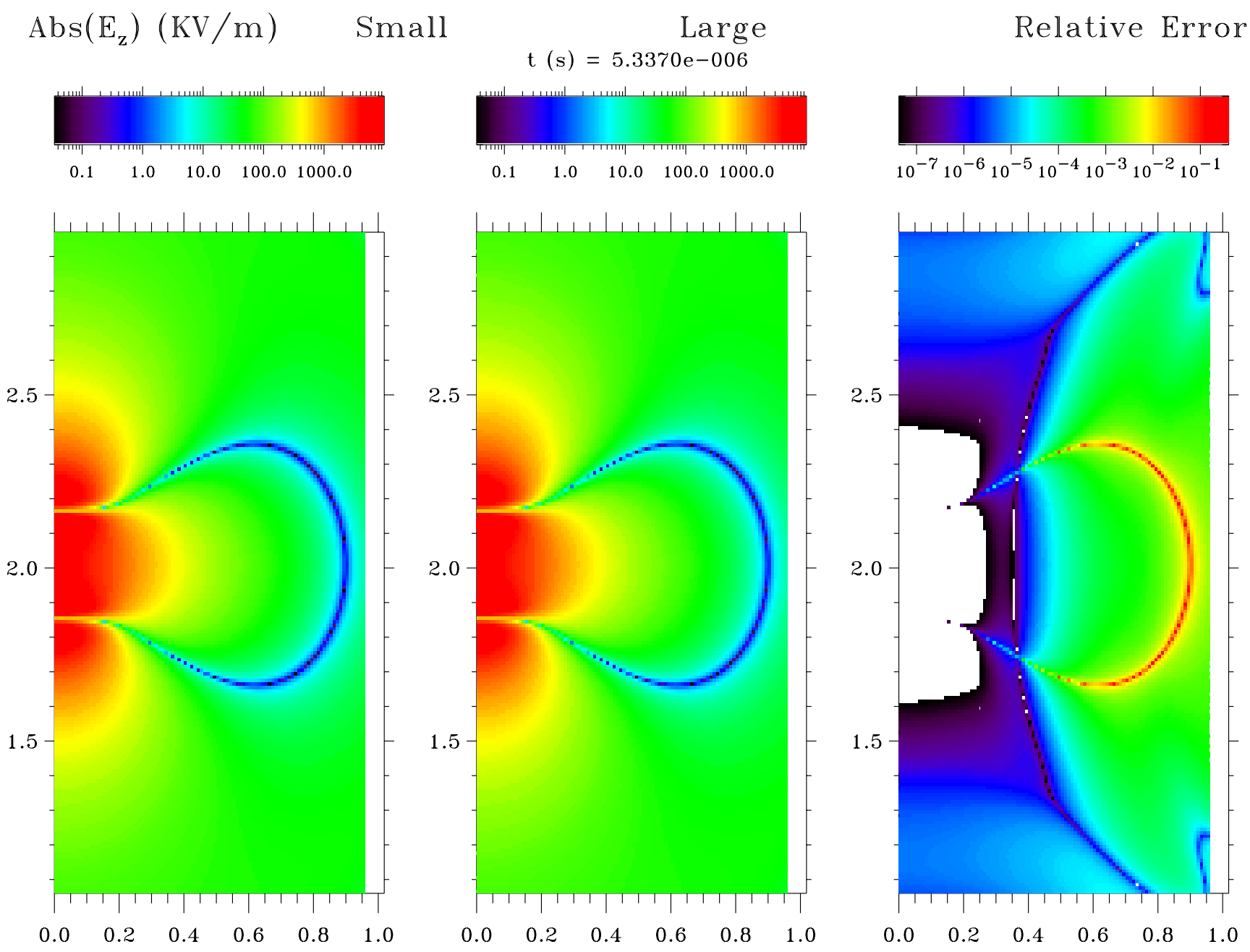
Abs(E_z) (KV/m)
Small
Large
Relative Error
t (s) = 5.3370e-006
0.1 1.0 10.0 100.0 1000.0
0.1 1.0 10.0 100.0 1000.0
10^-7 10^-6 10^-5 10^-4 10^-3 10^-2 10^-1
2.5
2.0
1.5
0.0 0.2 0.4 0.6 0.8 1.0

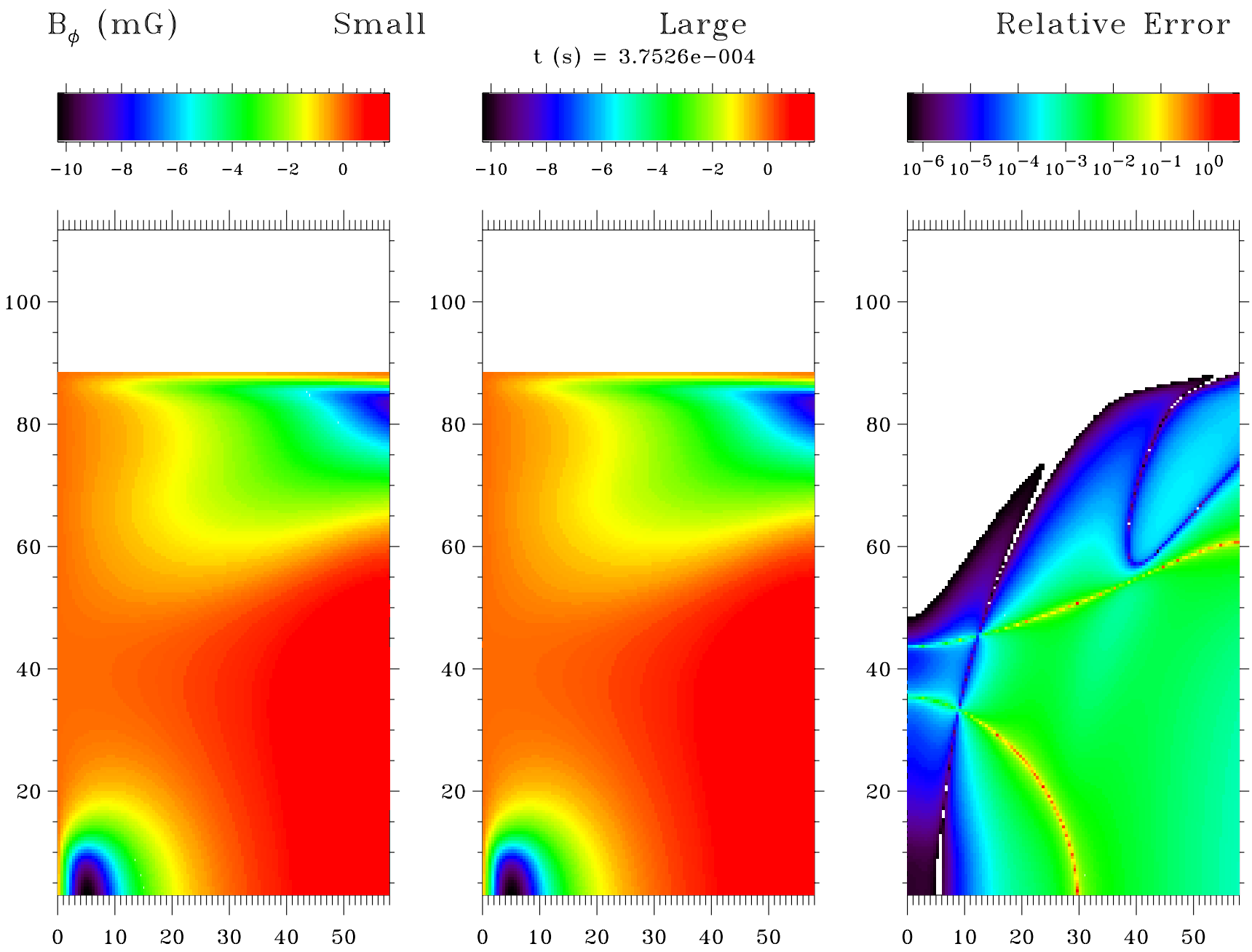
B_ϕ (mG)
Small
Large
Relative Error
t (s) = 3.7526e−004
−10 −8 −6 −4 −2 0
−10 −8 −6 −4 −2 0
10^{-6} 10^{-5} 10^{-4} 10^{-3} 10^{-2} 10^{-1} 10^{0}
100
80
60
40
20
0 10 20 30 40 50
100
80
60
40
20
0 10 20 30 40 50
100
80
60
40
20
0 10 20 30 40 50